ACS OMEGA

http://pubs.acs.org/journal/acsodf

Article

Photocatalytic Tandem Protocol for the Synthesis of Bis(indolyl)methanes using Cu-g-C_3N_4−Imine Decorated on TiO_2 Nanoparticles under Visible Light Irradiation

Maryam Ghanbari Kudeyani, Maasoumeh Jafarpour,* Narges Pourmorteza, and Abdolreza Rezaeifard*

Cite This: ACS Omega 2024, 9, 31344−31352

Read Online

ABSTRACT: In this article, the visible-light-assisted photocatalytic activity of TiO_2 nanoparticles functionalized with Cu(II) g−C_3N_4−imine was exploited for aerobic oxidation of alcohols to aldehydes followed by condensation with indoles in the presence of 2,2,6,6-tetramethylpiperidinyloxy to present a one-pot tandem strategy for the synthesis of bis(indolyl)methanes (BIMs) under solvent-free conditions. The synergistic effect between the components to improve the photocatalytic activity of the as-prepared Cu-g-C_3N_4−imine/TiO_2 nanoparticles resulting from electron−hole separation was approved by PL spectroscopy. Moreover, action spectra showed a light-dependent photocatalysis with effective visible-light responsivity of the photocatalyst. The present method includes different aspects of green chemistry: one-pot tandem synthesis of a variety of BIMs using alcohols that are less toxic, more available, more economical, and more stable than aldehydes; removing the byproducts resulting from overoxidation of alcohols and polymerization of aldehydes and indoles; the use of air as a safe oxidant; visible light as a safe energy source; and solvent-free conditions. A reusability test demonstrated that the catalyst retained its efficiency even after five runs.

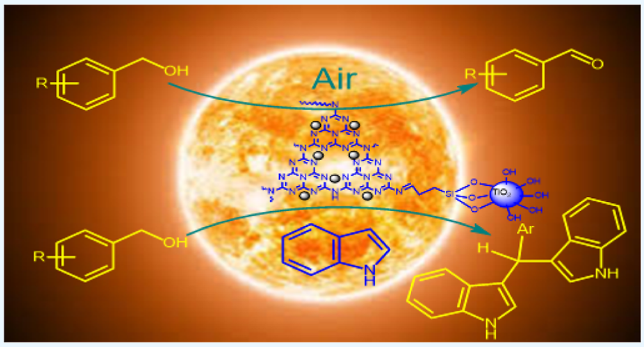

■ INTRODUCTION

The development of alternative strategies for efficient organic transformations based on the concept of "green sustainable chemistry" is greatly desired.[1−4] In this regard, photocatalytic or photoactivated reactions have rapidly developed in numerous areas of chemistry, such as organic synthesis. The mild reaction environment and renewable resources are advantages of this catalytic process, which make it a potential candidate for addressing many of the challenges of green chemistry.[5−8] Semiconductor-based photocatalytic materials have emerged as efficient and cost-effective materials for photocatalytic reactions. In this context, TiO_2 and its composites receive wide attention compared to other metal oxides because of their low cost, good stability, nontoxicity, chemical stability, and longer lifetime.[9,10] TiO_2 photocatalytic technology can only effectively utilize less than 6% of the energy derived from the sunlight incident to the earth's surface, which suggests its low potential for sustainable development in photocatalysis.[11−14] To address this problem, many modifications have been done on TiO_2 such as nonmetal and metal doping semiconductor compound modification and organic photosensitization.[15−20] Coupling of semiconductors or composites is an appropriate method to make photocatalysts effective in visible light for different applications.[21−25] In recent years, graphitic carbon nitride (g-C_3N_4) has become a rising star in the photocatalytic field. It is a stable metal-free photocatalyst that respondss to visible light.[26−30]

Just recently, we discovered visible-light-driven photocatalytic systems consisting of palladium[31] and cobalt,[32] incorporated in the g-C_3N_4−imine/TiO_2 nanohybrid. In the former, several types of transformations in a sequential one-pot strategy were promoted, including synchronous photocatalytic production of hydrogen and acceptorless synthesis of benzimidazoles, followed by photocatalytic olefin hydrogenation under mild reaction conditions.[31] The latter catalytic system showed a high photoefficiency toward aerobic oxidation of benzylic alcohols to aldehydes, followed by coupling with aromatic diamines to produce benzimidazoles under environmentally benign conditions.[32] Induced by the promising results of our previous works on g-C_3N_4−imine functionalized TiO_2 nanoparticles, herein we wish to present a new copper-containing photocatalyst that catalyzes one-pot tandem aerobic photooxidation of alcohols to aldehydes followed by

Received: November 12, 2023
Revised: April 2, 2024
Accepted: June 25, 2024
Published: July 11, 2024

https://doi.org/10.1021/acsomega.3c09007
ACS Omega 2024, 9, 31344−31352

Scheme 1. Cu(II)-g-C_3N_4−Imine/TiO_2 Nanohybrid-Catalyzed Aerobic Photooxidation of Benzylic Alcohols and Tandem Synthesis of Bis(indolyl)methanes Derivatives

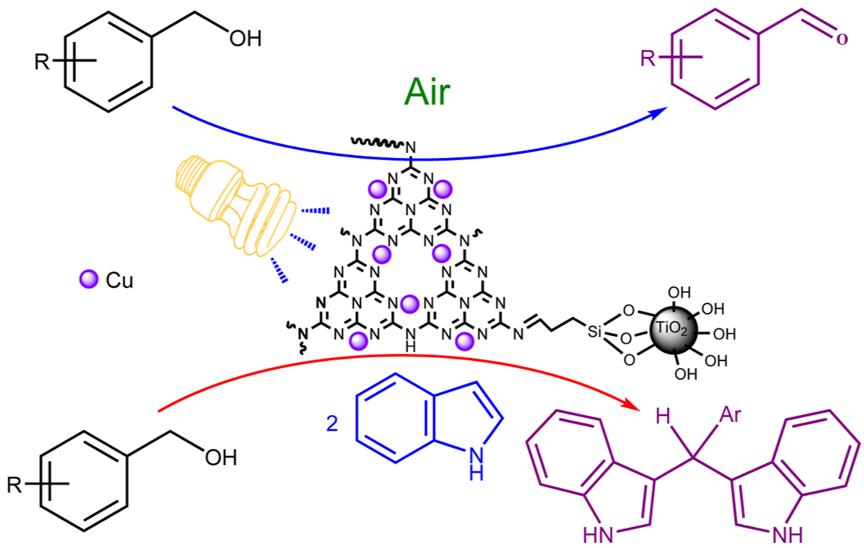

condensation with indoles in the presence of 2,2,6,6-tetramethylpiperidinyloxy (TEMPO) (Scheme 1) to produce bis(indolyl)methanes (BIMs) under solvent-free conditions. Among the catalytically important metals, copper has attracted great attention in organic reactions owing to its cheapness, abundance, and notable physical and chemical properties.[33] Copper compounds, combined with TEMPO, have long been known as highly effective catalysts for aerobic alcohol oxidation.[34,35] Nevertheless, their photocatalytic activity in the synthesis of N-heterocycles from alcohols has received less attention.

Heteroaromatic compounds have attracted a great deal of interest since more than half of the biologically active compounds produced by nature contain a heterocyclic moiety as a fundamental unit in their structure.[36,37] Particularly, indole derivatives are considered to be among the most important heterocyclic scaffolds due to their interesting biological and optical properties.[38,39] Among various indole derivatives, indole alkaloids substituted at C3, such as BIMs, received significant importance in the field of synthetic chemistry owing to their multiple biological relevance.[40,41] Antitumor,[42] anti-inflammatory,[43] and antihyperlipidemic activities are some of the therapeutic properties of these compounds.[44] Thus, the synthesis and functionalization of bis(indolyl)alkane derivatives have attracted significant attention, which led to many synthetic protocols. Although these strategies are useful, they are limited to specific classes of coupling partners in the presence of toxic metal salts, longer reaction times, low yields of products, high catalyst loadings, and high temperatures.[45−49] Alternatively, direct access to bis(indolyl)alkane derivatives from simple precursors such as alcohols would prove useful since they can be easily converted into aldehydes through oxidation reactions.

EXPERIMENTAL SECTION

Synthesis of Catalyst. The step-by-step preparation of the Cu-g-C_3N_4−imine/TiO_2 nanohybrid and experimental procedures are given in Supporting Information.

RESULTS AND DISCUSSION

Catalyst Fabrication and Structural Analysis. The synthesis of a TiO_2 immobilized Cu(II) Schiff base complex (Cu-g-C_3N_4−imine/TiO_2) is outlined in Scheme S1. The bulk g-C_3N_4 and TiO_2 nanoparticles were synthesized using hydrothermal methods.[31] The functionalized g-C_3N_4 (g-C_3N_4/imine) was prepared by the condensation of the $-NH_2$ group of g-C_3N_4 with organosilicon aldehyde in ethanol.[3] Then, the g-C_3N_4/imine compound attached to TiO_2, which gave the g-C_3N_4−imine/TiO_2 nanostructure. Finally, the desired complex, Cu-g-C_3N_4−imine/TiO_2, was synthesized by the reaction of g-C_3N_4−imine/TiO_2 and $Cu(OAc)_2$ H_2O in refluxing ethanol (Scheme S1, for experimental details, see the Supporting Information). The as-synthesized Cu-g-C_3N_4−imine/TiO_2 complex was characterized by XRD, FT-IR, FESEM, EDX, and elemental mapping.

The XRD patterns of TiO_2, g-C_3N_4, and Cu-g-C_3N_4−imine/TiO_2 are shown in Figure 1A. The diffraction peaks centered at 2θ = 25.4, 37.7, 48.2, and 54.1° correspond to the (101), (004), (200), and (105) crystal planes of anatase TiO_2, respectively (JCPDS no. 21-1272).[50] For g-C_3N_4, the peak at ∼13° with the plane (100) reveals the intraplanar structural packing of the aromatic system of g-C_3N_4, while the peak at 27.4° presents the stacking of the conjugated $\pi-\pi$ system that matches the (002) diffraction plane (JCPDS no. 87-1526).[51] The presence of peaks related to both components, g-C_3N_4 and TiO_2, in the XRD pattern of Cu-g-C_3N_4−imine/TiO_2 confirmed the successful fabrication of the title heterojunction composite. The peak at 13° to the (100) phase of g-C_3N_4 fades during the synthesis process due to the decreased planar size and structural defects.[52] Moreover, the broad peak at 22.5° is ascribed to SiO_2 in the heterostructure.

To determine the composition and chemical bonding of Cu-g-C_3N_4−imine/TiO_2, FT-IR spectra were tracked, as shown in Figure 1B. The typical band of TiO_2 at 450−750 cm^{-1} is related to the stretching vibrations of Ti−O groups [Figure 1B(a−c)].[53] In addition, the broad peaks attributed to the O−H bands and surface adsorbed water appeared at 1627 and 3400 cm^{-1}. For g-C_3N_4 [Figure 1B(b)], the sharp peak at 807 cm^{-1} shows the typical breathing mode of the triazine ring

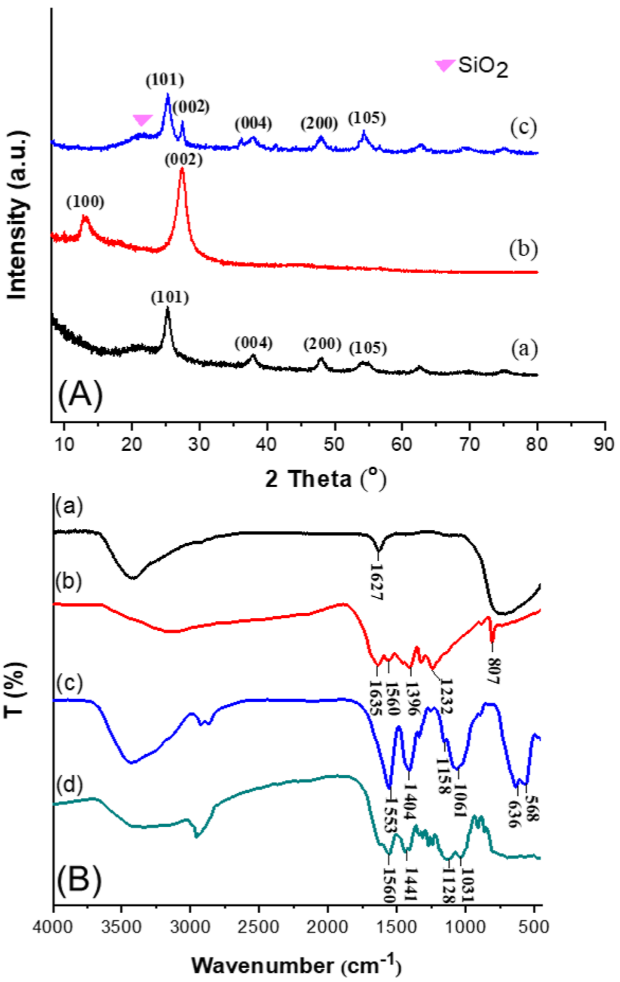

Figure 1. (A) XRD pattern of (a) TiO_2, (b) g-C_3N_4, and (c) Cu-g-C3N4−imine/TiO_2 nanohybrid. (B) FT-IR spectra of (a) nanostructure TiO_2, (b) g-C_3N_4, (c) g-C_3N_4−imine/TiO_2, and (d) Cu-g-C_3N_4−imine/TiO_2 nanohybrid.

system, and bands for stretching vibrations of C−N and C═N bonds in heterocycle rings appeared at 1232−1635 cm^{-1} region.[54] As depicted in Figure 1B(c), intense bands at 1061−1158 cm^{-1} rationalized stretching of Si−O bonds. In addition, the FT-IR patterns of g-C_3N_4 and TiO_2 appeared in Figure 1B(c,d), confirming their presence in the as-prepared composite.

The morphology of the as-prepared catalyst was identified by field-emission scanning electron microscopy (FE-SEM). The image depicted in Figure S1 showed uniform spherical nanoparticles with some aggregation and an average size of 19−22 nm.

EDX spectra and elemental mapping (Figure S1) confirmed the presence of Ti, O, Si, N, C, and Cu in the fabricated hybrid Cu-g-C_3N_4−imine/TiO_2 as well as the uniform distribution on the surface of TiO_2. The copper content in the catalyst was found to be 0.1 mmol g^{-1} based on inductively coupled plasma atomic emission spectroscopy.

TGA analysis was carried out to investigate the thermal behavior of the catalyst. The TGA thermogram of Cu-g-C_3N_4−imine/TiO_2 showed three stages of weight loss. The first stage ending at 250 °C is caused by losing the surface adsorbed water molecules. The stages ranging from 250 to 470 and 470−700 are attributed to the thermal decomposition of the organosilicon phase and g-C_3N_4, respectively. The TGA profile of Cu-g-C_3N_4−imine/TiO_2 showed that the catalyst is stable up to 300 °C (Figure S2).

Optical properties of TiO_2, g-C_3N_4, g-C_3N_4−imine, g-C_3N_4−imine/TiO_2, and Cu-g-C_3N_4−imine/TiO_2 composites were studied by UV−visible diffuse reflectance spectroscopy (Figure S3) and photoluminescence technique (PL)[55,56] (Figure 2). The band gap values determined by Tauc plots

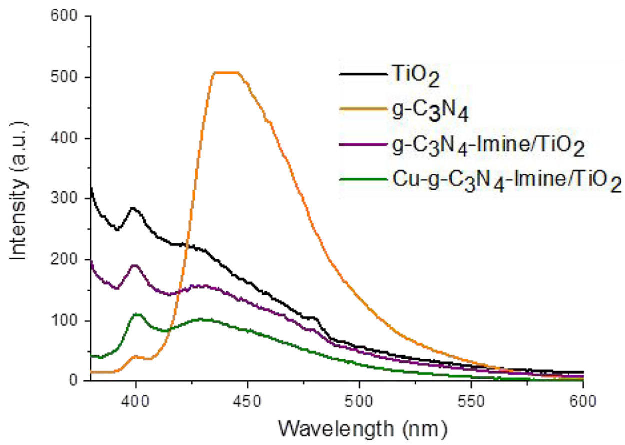

Figure 2. PL analysis of TiO_2, g-C_3N_4, g-C_3N_4−imine/TiO_2, and Cu-g-C_3N_4−imine/TiO_2.

(Figure S3) resulted in ∼3.15, 2.7, 2.9, 3, and 2.8 eV for TiO_2, g-C_3N_4, g-C_3N_4−imine, g-C_3N_4−imine/TiO_2, and Cu-g-C_3N_4−imine/TiO_2, respectively.

The results revealed that the as-prepared Cu-g-C_3N_4−imine/TiO_2 has the desired visible-light responsivity to boost the photocatalytic performance of Cu-g-C_3N_4−imine/TiO_2 (Figure S3). Moreover, the lower PL intensity of Cu-g-C_3N_4−imine/TiO_2 than those of its components, g-C_3N_4 and TiO_2 (Figure 2) revealed well that the decoration of TiO_2 with the g-C_3N_4−imine and Cu(II) reduces the electron−hole recombination, enhancing its photocatalytic activity.

■ CATALYTIC ACTIVITY ASSESSMENT

Aerobic Photooxidation of Benzylic Alcohols. The catalytic performance of the Cu-g-C_3N_4−imine/TiO_2 catalyst was investigated in the photo-oxidation of 4-chlorobenzyl alcohol (0.125 mmol) under visible light (CFL lamp) for the optimization of the reaction conditions. The results of the solvent effects, temperature, catalyst amount, nature of the radical producer, and oxidants on the oxidation of 4-chlorobenzyl alcohol (0.125 mmol) in the reaction vessel are given in Table S1. According to the experimental results, we found that solvent-free conditions were better for the reaction. Various solvents, including ethyl acetate, acetonitrile, ethanol, and water, produced low yields. The influence of temperature was studied in the photooxidation of 4-chlorobenzyl alcohol. With an increase in temperature from 25 to 70 °C, the yield of the product increased. According to Table S1 (entries 3, 10−12), the presence of a catalyst was inevitable for the reaction, and beyond the 2 mg of the catalyst, the catalytic performance decreased. The screening of the nature of the radical generator revealed a strong influence of TEMPO on the catalytic performance (Table S1, entries 3, 22−24). With only 0.01 mmol of TEMPO, the reaction was much faster, and the desired product was formed with an excellent yield of 98%

(Table S1, entry 3). The model reaction was also subjected to various oxidants such as TBHP, TBAOX, Oxone, UHP, H_2O_2, O_2, and air. The highest efficiency was obtained under the air itself as an oxidant (Table S1, entries 3, 16−21) at 70 °C when 2 mg of Cu−C_3N_4−imine/TiO_2 and 0.01 mmol of TEMPO under solvent-free and visible light (CFL lamp) conditions were used.

These optimized conditions were next applied to the aerobic oxidation of a variety of benzylic alcohols, and the results are summarized in Table 1. The different benzyl alcohols showed a relatively high tendency to aerobic oxidation in the presence of the title visible-light-responsive photocatalyst. However, the reaction performance is affected by the electronic demands of substrates. The unsubstituted benzyl alcohols or those substituted with electron-donating groups (Table 1, entries 1−8) were more reactive than those bearing electron-withdrawing groups (entry 9).

No ester and carboxylic acid products were detected, excluding any overoxidation of secondary and primary benzylic alcohols, respectively. The chemoselectivity of the method was notable. The primary benzylic alcohol-containing sulfide group (1f, entry 6), as well as cinnamyl alcohol as an allylic alcohol (1o, entry 15), oxidized selectively to the corresponding aldehydes, while sulfide and C═C moieties survived completely. Secondary benzyl alcohols (entries 10−14) were generally less reactive than primary ones (entries 1−9), most likely due to steric hindrance. Meanwhile, the aliphatic secondary alcohol adamantanol (entry 12) showed the least activity and acquired a low conversion of 32% after 240 min.

Photo-Induced Aerobic Tandem Synthesis of BIMs. To extend the scope of the present catalytic system, the catalytic potential of Cu-g-C_3N_4−imine/TiO_2 nanocomposite was exploited for the one-pot synthesis of various biologically important BIMs[38−44] from benzyl alcohols. The reaction of indole (0.26 mmol) with a variety of benzylic alcohols (0.125 mmol) in the presence of the Cu-g-C_3N_4−imine/TiO_2 nanocomposite and under the same reaction conditions used for oxidation of benzylic alcohols (vide supra) led to the formation of different C-3 alkylated bisindoles (Table 2). Inspection of the results in Table 2 revealed that the reaction rate was affected by the electronic demands of the substrates. Benzyl alcohols bearing electron-donating groups (such as −OMe, Me, and *t*-Butyl) accelerated the reaction, and pertinent bis(indolyl)methanes were produced in high yields within 4 h (Table 2, parts b,d,4e). Nevertheless, a strong electron-withdrawing nitro group on the phenyl ring of alcohol significantly retarded the reaction so that the product yield decreased to 52%, while a longer time of 6 h was applied (Table 2, 4i).

To confirm the superiority of the title photocatalyst, the catalytic activity of the parent and precursor materials was assessed in the aerobic oxidation of benzyl alcohols and the tandem synthesis of BIMs under the same conditions (Figure S4). Bare TiO_2, g-C_3N_4, g-C_3N_4−imine, g-C_3N_4−imine/TiO_2, Cu-g-C_3N_4, Cu-g-C_3N_4−imine, $Cu(OAc)_2$, and even the mixture of $Cu(OAc)_2$ and g-C_3N_4−imine/TiO_2 were inferior or quite ineffective. These results highlighted the synergistic effects of the catalyst precursors in the constructed photocatalyst for enhanced photocatalytic activity.

The recyclability of the catalyst was also studied for the oxidation of benzylic alcohols and the synthesis of BIMs under optimized conditions. After the completion of the reactions, the residual catalyst was removed by adding 2 mL of ethanol,

Table 1. Aerobic Oxidation of Benzylic Alcohols using the Cu-g-C_3N_4−imine/TiO_2/TEMPO System[a]

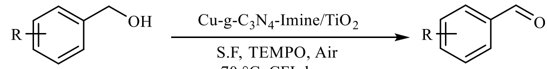

(1a-o) (2a-o)

Entry	Benzyl alcohols	Product[b]	Conversion[b] (Isolated Yield%)	Time(min)
1	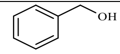 (1a)	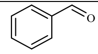 (2a)	90 (84)	75
2	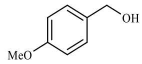 (1b)	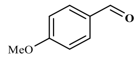 (2b)	95 (88)	90
3	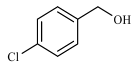 (1c)	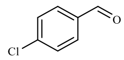 (2c)	98 (93)	75
4	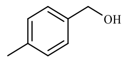 (1d)	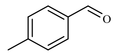 (2d)	96 (87)	80
5	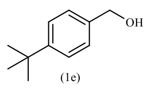 (1e)	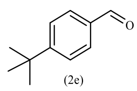 (2e)	97 (90)	120
6	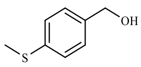 (1f)	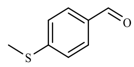 (2f)	85 (78)	180
7	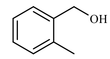 (1g)	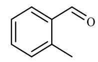 (2g)	95 (89)	90
8	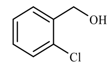 (1h)	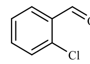 (2h)	98 (93)	90
9	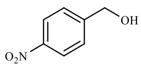 (1i)	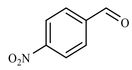 (2i)	75 (68)	180
10	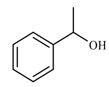 (1j)	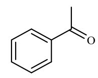 (2j)	95 (88)	75
11	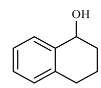 (1k)	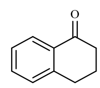 (2k)	70 (59)	240
12	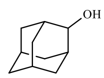 (1l)	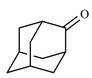 (2l)	32	240
13	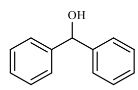 (1m)	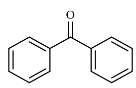 (2m)	79 (70)	240
14	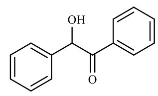 (1n)	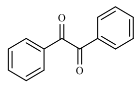 (2n)	82 (75)	180
15	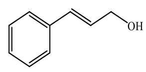 (1o)	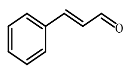 (2o)	52 (43)	240

https://doi.org/10.1021/acsomega.3c09007
ACS Omega 2024, 9, 31344−31352

Table 1. continued

[a]An aerobic solvent-free condition was used for running the reactions at 70 °C using the substrate (0.125 mmol), TEMPO (0.01 mmol), and catalyst (2 mg) under CFL lamp as an energy source. [b]The products were identified by NMR spectra. [c]GC yield. The selectivity of products was >99% based on GC analysis.

followed by centrifugation, and then dried under a vacuum to be used for the next run. The catalyst was reusable for five runs with no noticeable loss of activity (Figure S5). Moreover, a comparison of the FT-IR spectra of the fresh and reused catalyst revealed that Cu-g-C_3N_4−imine/TiO_2 preserved its structure during the oxidation reaction and synthesis of BIM (Figure S6).

Photocatalytic Assessment. To better understand the enhancement of the catalytic performance that occurs through light irradiation of Cu-g-C_3N_4−imine/TiO_2, wavelength screening was carried out using different light sources (Figure 3). For this purpose, the contribution of light in the oxidation of 4-chlorobenzyl and tandem synthesis of BIMs by different light sources (Supporting Information) was investigated (Figure 3). As can be seen in Figure 3a, in both reactions, CFL light rendered the greater irradiation contribution to the overall conversion rate, and thus, the visible light dependence of the reaction was proved. The proposed mechanism depicted in Scheme S2 (Supporting Information) shows the photocatalytic effects of the TiO_2 core and g-C_3N_4 on the efficiency of Cu-g-C_3N_4−imine/TiO_2 in this reaction system. It should be noted that in the dark, the reaction proceeded by only 20%, indicating a thermal contribution.

Then, screening of different irradiation wavelengths for the oxidation of 4-chlorobenzyl alcohol, as well as the synthesis of the related BIMs, was carried out under a 40 W CFL bulb equipped with cutoff filters to exclude any radiation below 400

Table 2. Substrate Scope for C-3 Alkylation of Indole with Alcohols[a]

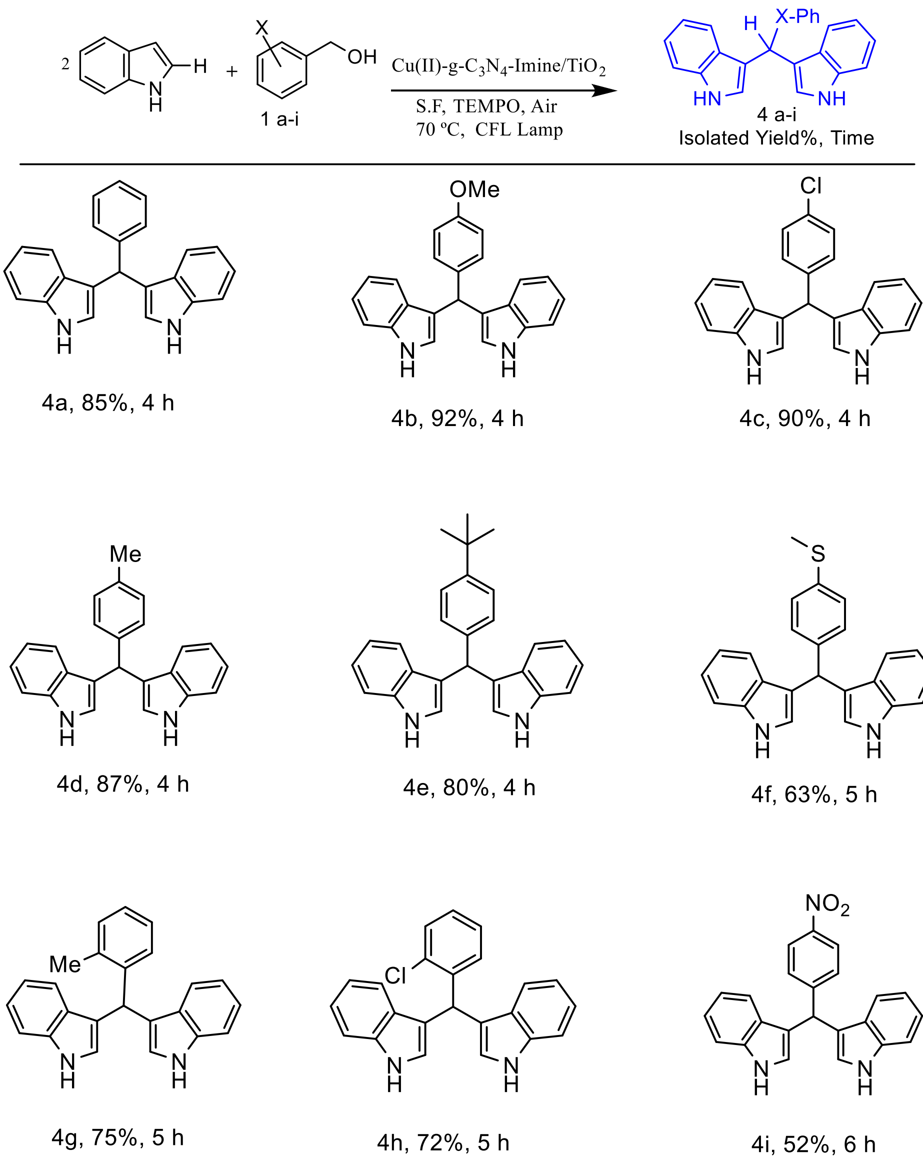

[a]Reaction condition: indole (0.26 mmol) and benzyl alcohol (0.125 mmol) by Cu-g-C_3N_4−imine/TiO_2 alcohol (2 mg) using TEMPO (2 mg) at 70 °C under air and visible light (CFL lamp).

https://doi.org/10.1021/acsomega.3c09007
ACS Omega 2024, 9, 31344−31352

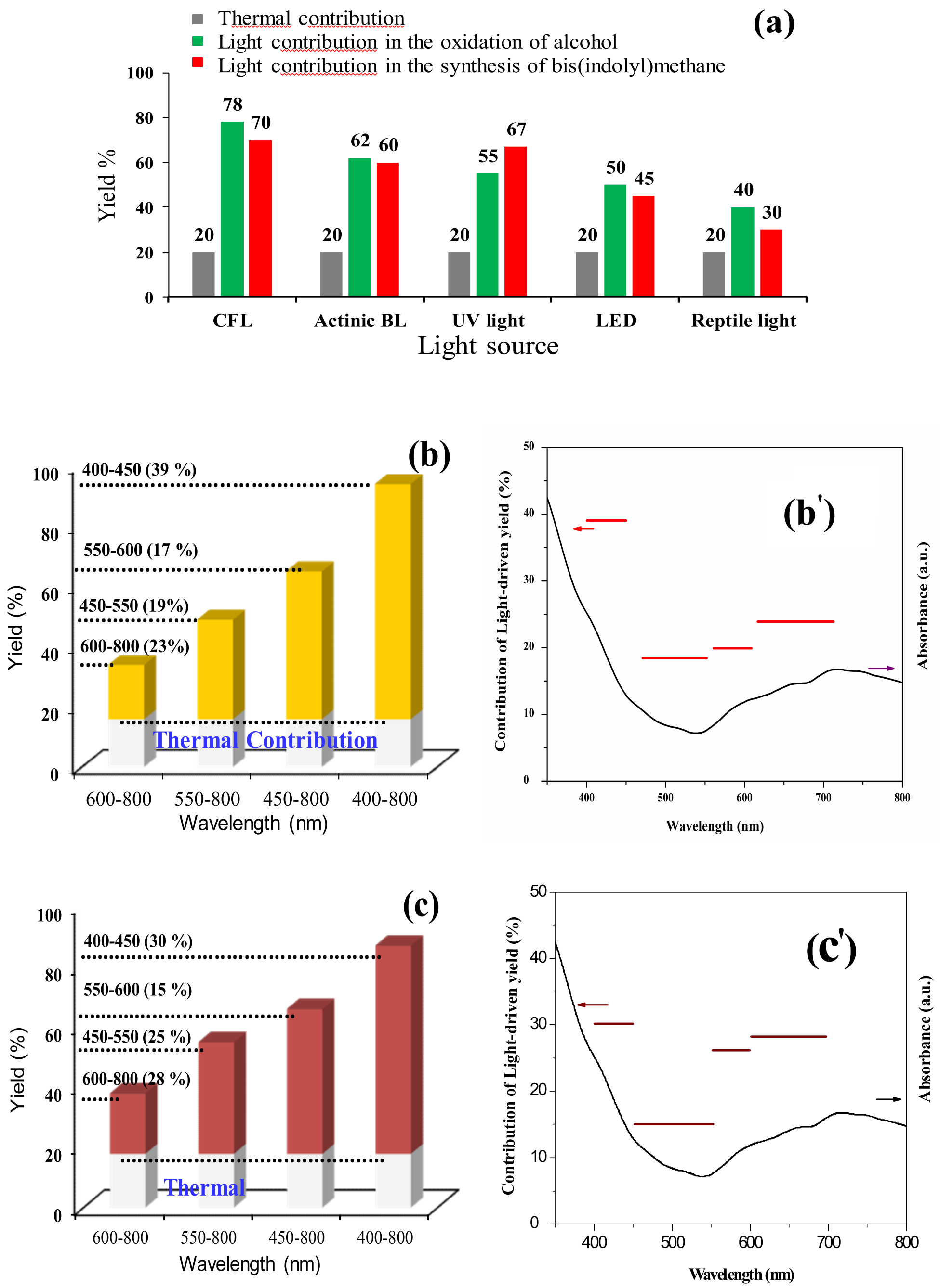

Figure 3. Dependence of the catalytic activity of Cu-g-C_3N_4–imine/TiO_2 for (a) oxidation of benzylic alcohols and synthesis of BIMs on the irradiation wavelength under different light sources. Dependence of the catalytic activity of Cu-g-C_3N_4–imine/TiO_2 for (b,b′) oxidation of benzylic alcohols and (c,c′) synthesis of BIMs on irradiation wavelength.

nm to ensure that only visible light irradiates the reaction (Figure 3b,b′,c,ĉ). Without a filter, 4-chlorobenzyl alcohol conversion can reach 98%. Employing a 450–800 nm filter, the conversion decreased to 67%. Similarly, the light with a wavelength range of 550–800 and 600–800 nm filters gave 4-chlorobenzyl alcohol conversions of 53 and 38%, respectively. By deducting the contribution of the thermal reaction, we can get the contribution of irradiation that is 39, 17, 19, and 23% for 400–450, 450–550, 550–600, and 600–800 nm, respectively (Figure 3b). Moreover, a similar trend was obtained for the synthesis of BIMs from 4-chlorobenzyl alcohol with 90, 69, 58, and 40% yield relative to the above-mentioned wavelength ranges, and the contributions of irradiation in these cases are 30, 15, 25, and 28%, respectively (Figure 3c).

These results agree well with the UV–vis absorption spectrum of the Cu-g-C_3N_4–imine/TiO_2 catalyst (Figure S3). Finally, to confirm the light dependency of the as-prepared catalyst, an action spectrum was also screened. In this regard, the reaction rate of the oxidation of 4-chlorobenzyl alcohol, as well as the formation of the pertinent BIM using Cu-g-C_3N_4–imine/TiO_2 under irradiation with different wavelengths, was investigated. As shown in Figure 4, a good correlation is observed between apparent quantum yields[57] and the diffuse reflectance spectrum of the nanocatalyst, which confirms that the reactions are taking place photocatalytically.

https://doi.org/10.1021/acsomega.3c09007
ACS Omega 2024, 9, 31344–31352

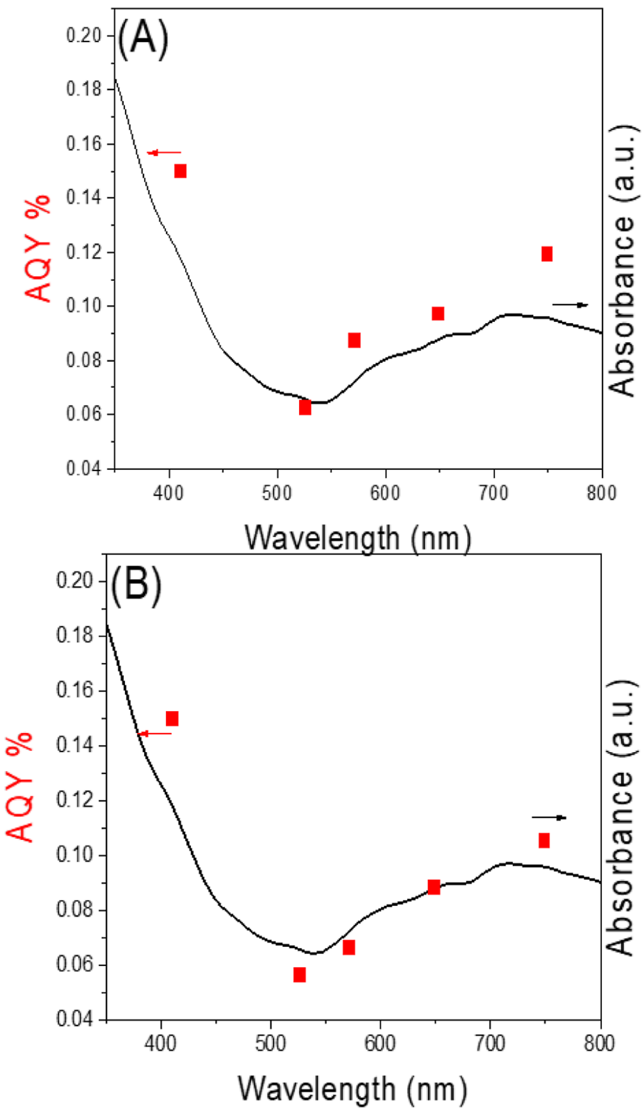

Figure 4. Action spectrum for the oxidation of (A) 4-chlorobenzyl alcohol and (B) synthesis of BIMs from 4-chlorobenzyl alcohol and indole using Cu-g-C_3N_4−imine/TiO_2 photocatalyst in the optimized reaction condition.

CONCLUSIONS

In conclusion, the band gap of TiO_2 nanoparticles modified by Cu-g-C_3N_4−imine induced outstanding photocatalytic activity in aerobic oxidation of benzylic alcohols and tandem synthesis of BIMs under visible light. An unexpected result of this aerobic method is that a variety of BIMs can be prepared in the presence of visible light without any byproducts such as overoxidation alcohols or polymerization of aldehydes and indoles. The light-dependent photocatalysis and effective visible-light responsivity of the photocatalyst were approved by action spectra. PL spectra revealed the effective separation of carriers in the fabricated catalyst, promoting its photocatalytic activity. The developed synthesis protocol proceeds with the merits of mild conditions, broad substrate scope, operational simplicity, and high atom efficiency, with an eco-energy source under solvent-free conditions and air as an ideal oxidant. Also, the reusability and durability of the title active catalyst that uses a low catalyst loading are the strengths of the presented work.

ASSOCIATED CONTENT

Supporting Information

The Supporting Information is available free of charge at https://pubs.acs.org/doi/10.1021/acsomega.3c09007.

Instrumentation, experimental synthetic procedures, additional analyses of photocatalyst used in this work, proposed mechanism, and spectral and optimization data (PDF)

AUTHOR INFORMATION

Corresponding Authors

Maasoumeh Jafarpour − *Catalysis Research Laboratory, Department of Chemistry, Faculty of Science, University of Birjand, Birjand 97179-414, Iran;* orcid.org/0000-0002-9946-5013; Email: mjafarpour@birjand.ac.ir, jafarpouryas@gmail.com

Abdolreza Rezaeifard − *Catalysis Research Laboratory, Department of Chemistry, Faculty of Science, University of Birjand, Birjand 97179-414, Iran;* orcid.org/0000-0002-8717-9036; Email: rrezaeifard@birjand.ac.ir, rrezaeifard@gmail.com

Authors

Maryam Ghanbari Kudeyani − *Catalysis Research Laboratory, Department of Chemistry, Faculty of Science, University of Birjand, Birjand 97179-414, Iran*

Narges Pourmorteza − *Catalysis Research Laboratory, Department of Chemistry, Faculty of Science, University of Birjand, Birjand 97179-414, Iran*

Complete contact information is available at: https://pubs.acs.org/10.1021/acsomega.3c09007

Notes

The authors declare no competing financial interest.

ACKNOWLEDGMENTS

Support for this work by the Research Council of the University of Birjand is appreciated.

REFERENCES

(1) Zuin, V. G.; Eilks, I.; Elschami, M.; Kümmerer, K. Education in green chemistry and in sustainable chemistry: perspectives towards sustainability. *Green Chem.* **2021**, *23* (4), 1594−1608.

(2) Itoh, T.; Takagi, Y. Laccase-catalyzed reactions in ionic liquids for green sustainable chemistry. *ACS Sustainable Chem. Eng.* **2021**, *9* (4), 1443−1458.

(3) Yoo, W. J.; Ishitani, H.; Saito, Y.; Laroche, B.; Kobayashi, S. Reworking organic synthesis for the modern age: Synthetic strategies based on continuous-flow addition and condensation reactions with heterogeneous catalysts. *J. Org. Chem.* **2020**, *85* (8), 5132−5145.

(4) Yesmin, S.; Abbas, S. J.; Ke, S. C. A powerful and multifunctional catalyst for organic synthesis, transformation, and environmental remediation: A polyImidazole supported trimetallic catalyst. *Appl. Catal., B* **2022**, *316*, 121629.

(5) Lin, Y.; Guo, J.; San Martin, J.; Han, C.; Martinez, R.; Yan, Y. Photoredox organic synthesis employing heterogeneous photocatalysts with emphasis on halide perovskite. *Chem-Eur Jl* **2020**, *26* (58), 13118−13136.

(6) Akhundi, A.; Badiei, A.; Ziarani, G. M.; Habibi-Yangjeh, A.; Munoz-Batista, M. J.; Luque, R. Graphitic carbon nitride-based photocatalysts: toward efficient organic transformation for value-added chemicals production. *Mol. Catal.* **2020**, *488*, 110902.

(7) Qiu, X.; Zhang, Y.; Zhu, Y.; Long, C.; Su, L.; Liu, S.; Tang, Z. Applications of nanomaterials in asymmetric photocatalysis: recent

progress, challenges, and opportunities. *Adv. Mater.* **2021**, *33* (6), 2001731.

(8) Qi, M. Y.; Conte, M.; Anpo, M.; Tang, Z. R.; Xu, Y. J. Cooperative coupling of oxidative organic synthesis and hydrogen production over semiconductor-based photocatalysts. *Chem. Rev.* **2021**, *121* (21), 13051−13085.

(9) Haruna, A.; Chong, F. K.; Ho, Y. C.; Merican, Z. M. A. Preparation and modification methods of defective titanium dioxide-based nanoparticles for photocatalytic wastewater treatment—a comprehensive review. *Environ. Sci. Pollut. Res.* **2022**, *29*, 70706−70745.

(10) Bhosale, R.; Debnath, B.; Ogale, S. Designing Nanoengineered Photocatalysts for Hydrogen Generation by Water Splitting and Conversion of Carbon Dioxide to Clean Fuels. *Chem. Rec.* **2022**, *22*, No. e202200110.

(11) Singh, R.; Dutta, S. A review on H2 production through photocatalytic reactions using TiO_2/TiO_2-assisted catalysts. *Fuel* **2018**, *220*, 607−620.

(12) Luo, J.; Zhang, S.; Sun, M.; Yang, L.; Luo, S.; Crittenden, J. C. A critical review on energy conversion and environmental remediation of photocatalysts with remodeling crystal lattice, surface, and interface. *ACS Nano* **2019**, *13* (9), 9811−9840.

(13) Kumar, A.; Choudhary, P.; Kumar, A.; Camargo, P. H.; Krishnan, V. Recent advances in plasmonic photocatalysis based on TiO2 and noble metal nanoparticles for energy conversion, environmental remediation, and organic synthesis. *Small* **2022**, *18* (1), 2101638.

(14) Kumaravel, V.; Mathew, S.; Bartlett, J.; Pillai, S. C. Photocatalytic hydrogen production using metal doped TiO2: A review of recent advances. *Appl. Catal., B* **2019**, *244*, 1021−1064.

(15) Shayegan, Z.; Lee, C. S.; Haghighat, F. TiO_2 photocatalyst for removal of volatile organic compounds in gas phase−A review. *Chem. Eng. J.* **2018**, *334*, 2408−2439.

(16) Ziental, D.; Czarczynska-Goslinska, B.; Mlynarczyk, D. T.; Glowacka-Sobotta, A.; Stanisz, B.; Goslinski, T.; Sobotta, L. Titanium dioxide nanoparticles: prospects and applications in medicine. *Nanomaterials* **2020**, *10* (2), 387.

(17) Sulaiman, S. N. A.; Noh, M. Z.; Adnan, N. N.; Bidin, N.; Ab Razak, S. N. Effects of photocatalytic activity of metal and non-metal doped $Tio_2$for Hydrogen production enhancement - A Review. *J. Phys.: Conf. Ser.* **2018**, *1027* (1), 012006.

(18) Moma, J.; Baloyi, J. Modified titanium dioxide for photocatalytic applications; In *Photocatalysts-Applications and Attributes*; Khan, S. B., Akhtar, K., Eds.; IntechOpen, 2019; Vol. *18*, pp 10−5772.

(19) Chen, J.; Qiu, F.; Xu, W.; Cao, S.; Zhu, H. Recent progress in enhancing photocatalytic efficiency of TiO2-based materials. *Appl. Catal., A* **2015**, *495*, 131−140.

(20) Mittal, A.; Mari, B.; Sharma, S.; Kumari, V.; Maken, S.; Kumari, K.; Kumar, N. Non-metal modified TiO_2: A step towards visible light photocatalysis. *J. Mater. Sci.: Mater. Electron.* **2019**, *30* (4), 3186−3207.

(21) Ghattavi, S.; Nezamzadeh-Ejhieh, A. A visible light driven AgBr/g-C3N4 photocatalyst composite in methyl orange photodegradation: focus on photoluminescence, mole ratio, synthesis method of g-C3N4 and scavengers. *Composites, Part B* **2020**, *183*, 107712.

(22) Puga, F.; Navío, J.; Hidalgo, M. C. Enhanced UV and visible light photocatalytic properties of synthesized AgBr/SnO_2 composites. *Sep. Purif. Technol.* **2021**, *257*, 117948.

(23) Wang, J.; Zhang, D.; Deng, J.; Chen, S. Fabrication of phosphorus nanostructures/TiO2 composite photocatalyst with enhancing photodegradation and hydrogen production from water under visible light. *J. Colloid Interface Sci.* **2018**, *516*, 215−223.

(24) Du, Z.; Cheng, C.; Tan, L.; Lan, J.; Jiang, S.; Zhao, L.; Guo, R. Enhanced photocatalytic activity of Bi2WO6/TiO2 composite coated polyester fabric under visible light irradiation. *Appl. Surf. Sci.* **2018**, *435*, 626−634.

(25) Khan, A. A.; Tahir, M. Well-designed 2D/2D Ti3C2TA/R MXene coupled g-C3N4 heterojunction with in-situ growth of anatase/rutile TiO_2 nucleates to boost photocatalytic dry-reforming of methane (DRM) for syngas production under visible light. *Appl. Catal., B* **2021**, *285*, 119777.

(26) Wang, S.; Zhang, J.; Li, B.; Sun, H.; Wang, S. Engineered graphitic carbon nitride-based photocatalysts for visible-light-driven water splitting: a review. *Energy Fuels* **2021**, *35* (8), 6504−6526.

(27) Shi, Y.; Li, L.; Xu, Z.; Sun, H.; Guo, F.; Shi, W. One-step simple green method to prepare carbon-doped graphitic carbon nitride nanosheets for boosting visible-light photocatalytic degradation of tetracycline. *J. Chem. Technol. Biotechnol.* **2021**, *96* (11), 3122−3133.

(28) Ren, Y.; Zeng, D.; Ong, W. J. Interfacial engineering of graphitic carbon nitride (g-C_3N_4)-based metal sulfide heterojunction photocatalysts for energy conversion: a review. *Chin. J. Catal.* **2019**, *40* (3), 289−319.

(29) Hong, Y.; Liu, E.; Shi, J.; Lin, X.; Sheng, L.; Zhang, M.; Wang, L.; Chen, J. A direct one-step synthesis of ultrathin g-C3N4 nanosheets from thiourea for boosting solar photocatalytic H2 evolution. *Int. J. Hydrogen Energy* **2019**, *44* (14), 7194−7204.

(30) Low, S. S.; Chen, Z.; Li, Y.; Lu, Y.; Liu, Q. Design principle in biosensing: Critical analysis based on graphitic carbon nitride (G-C3N4) photoelectrochemical biosensor. *TrAC, Trends Anal. Chem.* **2021**, *145*, 116454.

(31) Jafarpour, M.; Feizpour, F.; Rezaeifard, A.; Pourmorteza, N.; Breit, B. Tandem photocatalysis protocol for hydrogen generation/olefin hydrogenation using Pd-g-C3N4-Imine/TiO2 nanoparticles. *Inorg. Chem.* **2021**, *60* (13), 9484−9495.

(32) Pourmorteza, N.; Jafarpour, M.; Feizpour, F.; Rezaeifard, A. TiO_2 nanoparticles decorated with Co-Schiff base-g-C_3N_4 as an efficient photocatalyst for one-pot visible light-assisted synthesis of benzimidazoles. *RSC Adv.* **2022**, *12* (35), 22526−22541.

(33) Silva, T. F. S.; Martins, L. M. D. R. S. Recent Advances in Copper Catalyzed Alcohol Oxidation in Homogeneous Medium. *Molecules* **2020**, *25*, 748−762.

(34) Sasano, Y.; Iwabuchi, Y. Copper-Catalyzed Aerobic Oxidation of Alcohols; In *Science of Synthesis*; Bagley, M. C., Ed.; Georg Thieme Verlag, 2023; Vol. *5*, pp 325−359..

(35) Cardona, F., Parmeggiani, C., Eds.; *Transition Metal Catalysis in Aerobic Alcohol Oxidation*; Royal Society of Chemistry: Cambridge, 2015.

(36) Perrone, S.; Troisi, L.; Salomone, A. Heterocycle Synthesis through Pd-Catalyzed Carbonylative Coupling. *Eur. J. Org Chem.* **2019**, *2019* (29), 4626−4643.

(37) Guillemard, L.; Kaplaneris, N.; Ackermann, L.; Johansson, M. J. Late-stage C−H functionalization offers new opportunities in drug discovery. *Nat. Rev. Chem* **2021**, *5* (8), 522−545.

(38) Dhuguru, J.; Skouta, R. Role of indole scaffolds as pharmacophores in the development of anti-lung cancer agents. *Molecules* **2020**, *25* (7), 1615.

(39) El-Sharief, A. M. S.; Ammar, Y. A.; Belal, A.; El-Sharief, M. A. S.; Mohamed, Y. A.; Mehany, A. B.; Elhag Ali, G. A.; Ragab, A. Design, synthesis, molecular docking and biological activity evaluation of some novel indole derivatives as potent anticancer active agents and apoptosis inducers. *Bioorg. Chem.* **2019**, *85*, 399−412.

(40) Sai Manoj Gorantla, N. V. T.; Guruprasad Reddy, P.; Abdul Shakoor, S. M.; Mandal, R.; Roy, S.; Mondal, K. C. Tetranuclear 3d/4f Coordination Complexes as Homogeneous Catalysts for Bis (indolyl) methane Syntheses. *ChemistrySelect* **2019**, *4* (26), 7722−7727.

(41) Mathavan, S.; Kannan, K.; Yamajala, R. B. Thiamine hydrochloride as a recyclable organocatalyst for the synthesis of bis (indolyl) methanes, tris (indolyl) methanes, 3, 3-di (indol-3-yl) indolin-2-ones and biscoumarins. *Org. Biomol. Chem.* **2019**, *17* (44), 9620−9626.

(42) Li, M. X.; Pu, X. J.; Zhang, X.; Zheng, X.; Gao, H.; Xiao, W. L.; Wan, C. P.; Mao, Z. W. Synthesis and Biological Evaluation of Heterocyclic Substituted Bis (indolyl) methanes. *Curr. Org. Synth.* **2020**, *17* (2), 144−150.

(43) Nagre, D. T.; Mali, S. N.; Thorat, B. R.; Thorat, S. A.; Chopade, A. R.; Farooqui, M.; Agrawal, B. Synthesis, In-Silico Potential

Enzymatic Target Predictions, Pharmacokinetics, Toxicity, Anti-Microbial and Anti-Inflammatory Studies of Bis-(2-Methylindolyl) Methane Derivatives. *Curr. Enzyme Inhib.* **2021**, *17* (2), 127−143.

(44) Rivas-Loaiza, J. A.; García-Merinos, J. P.; Ramírez-Díaz, M. I.; López-Ruiz, H.; López, Y. Synthesis of Bis (indolyl) methanes via thiourea organocatalysts carrying 3, 5-bis (trifluoromethyl) phenyl or 3, 5-dichlorophenyl moieties. *J. Mol. Struct.* **2022**, *1264*, 133209.

(45) Biswas, N.; Sharma, R.; Srimani, D. Ruthenium Pincer Complex Catalyzed Selective Synthesis of C-3 Alkylated Indoles and Bisindolylmethanes Directly from Indoles and Alcohols. *Adv. Synth. Catal.* **2020**, *362* (14), 2902−2910.

(46) Zhang, R.; Ma, R.; Chen, R.; Wang, L.; Ma, Y. Regioselective C3Alkylation of Indoles for the Synthesis of Bis(indolyl)methanes and 3-Styryl Indoles. *J. Org. Chem.* **2024**, *89* (3), 1846−1857.

(47) Taya, N.; Agarwal, J. Unmodified 'chitosan in water' as an efficient and recyclable heterogeneous catalytic system for the synthesis of bis(indolyl)methanes. *Appl. Catal., A* **2024**, *670*, 119539.

(48) Athavale, R.; Gardi, S.; Choudhary, F.; Patil, D.; Chandan, N.; More, P. Novel acidic ionic liquid [BEMIM] [HSO_4]: A highly efficient and recyclable catalyst for the synthesis of bis-indolyl methane derivatives. *Appl. Catal., A* **2024**, *669*, 119505.

(49) Nguyen, H. Y.; Tran, Th. H.; Do, H. N.; Van Do, D.; Ngo, Q. A.; Tien, N. Q.; Thanh Nga, T. T.; Nguyen, H.; Hung, T. Q.; Dang, T. T. LiOtBu-promoted synthesis of bis(3-indolyl)methanes by the alkylation of indoles with alcohols under air. *RSC Adv.* **2024**, *14*, 2341−2345.

(50) Nasr, M.; Abou Chaaya, A.; Abboud, N.; Bechelany, M.; Viter, R.; Eid, C.; Khoury, A.; Miele, P. Photoluminescence: A very sensitive tool to detect the presence of anatase in rutile phase electrospun TiO2 nanofibers. *Superlattices Microstruct.* **2015**, *77*, 18−24.

(51) Xing, Y.; Yin, L.; Zhao, Y.; Du, Z.; Tan, H. Q.; Qin, X.; Ho, W.; Qiu, T.; Li, Y. G. Construction of the 1D covalent organic framework/2D g-C3N4 heterojunction with high apparent quantum efficiency at 500 nm. *ACS Appl. Mater. Interfaces* **2020**, *12* (46), 51555−51562.

(52) Yang, S.; Gong, Y.; Zhang, J.; Zhan, L.; Ma, L.; Fang, Z.; Vajtai, R.; Wang, X.; Ajayan, P. M. Exfoliated Graphitic Carbon Nitride Nanosheets as Efficient Catalysts for Hydrogen Evolution Under Visible Light. *Adv. Mater.* **2013**, *25*, 2452−2456.

(53) Rasalingam, S.; Wu, C. M.; Koodali, R. T. Modulation of pore sizes of titanium dioxide photocatalysts by a facile template free hydrothermal synthesis method: implications for photocatalytic degradation of rhodamine B. *ACS Appl. Mater. Interfaces* **2015**, *7* (7), 4368−4380.

(54) He, Y.; Zhang, L.; Teng, B.; Fan, M. New application of Z-scheme $Ag_3PO_4/g\text{-}C_3N_4$ composite in converting CO_2 to fuel. *Environ. Sci. Technol.* **2015**, *49* (1), 649−656.

(55) Chang, F.; Zhao, Sh.; Lei, Y.; Wang, X.; Dong, F.; Zhu, G.; Kong, Y. Jointly augmented photocatalytic Jointly augmented photocatalytic NO removal by S-scheme Bi12SiO20/Ag2MoO4 heterojunctions with surface oxygen vacanciesremoval by S-scheme $Bi_{12}SiO_{20}$/ Ag_2MoO_4 heterojunctions with surface oxygen vacancies. *J. Colloid Interface Sci.* **2023**, *649*, 713−723.

(56) Chang, F.; Zhao, Sh.; Lei, Y.; Peng, Sh.; Liu, D.; Kong, Y. Ball-milling fabrication of n-p heterojunctions $Bi_4O_5Br_2/\alpha$-MnS with strengthened photocatalytic removal of bisphenol A in a Z-Scheme model. *Sep. Purif. Technol.* **2023**, *304*, 122324.

(57) Zhao, Y.; Zhang, P.; Yang, Z.; Li, L.; Gao, J.; Chen, S.; Xie, T.; Diao, C.; Xi, S.; Xiao, B.; et al. Mechanistic analysis of multiple processes controlling solar-driven H_2O_2 synthesis using engineered polymeric carbon nitride. *Nat. Commun.* **2021**, *12* (1), 3701.

https://doi.org/10.1021/acsomega.3c09007
ACS Omega 2024, 9, 31344−31352